Scale-based fuzzy connectivity: a novel image segmentation methodology and its validation

Punam K. Saha, Jayaram K. Udupa

Medical Image Processing Group, Department of Radiology,
University of Pennsylvania, Philadelphia, PA 19104

ABSTRACT

This paper extends a previously reported theory and algorithms for fuzzy connected object definition. It introduces "object scale" for determining the neighborhood size for defining affinity, the degree of local hanging togetherness between image elements. Object scale allows us to use a varying neighborhood size in different parts of the image. This paper argues that scale-based fuzzy connectivity is natural in object definition and demonstrates that this leads to a more effective object segmentation than without using scale in fuzzy connectedness. Affinity is described as consisting of a homogeneity-based and an object-feature-based component. Families of non scale-based and scale-based affinity relations are constructed. An effective method for giving a rough estimate of scale at different locations in the image is presented. The original theoretical and algorithmic framework remains more-or-less the same but considerably improved segmentations result. A quantitative statistical comparison between the non scale-based and the scale-based methods was made based on phantom images generated from patient MR brain studies by first segmenting the objects, and then by adding noise and blurring, and background component. Both the statistical and the subjective tests clearly indicate the superiority of scale-based method in capturing details and in robustness to noise.

Keywords: Image analysis, Fuzzy topology, Segmentation, Scale, Connectivity

1. INTRODUCTION

Most real objects have a heterogeneous material composition. Further, imaging devices have inherent limitations including spatial, parametric, and temporal resolutions. In the acquired images of objects, these introduce inaccuracies and artifacts such as noise, blurring, and background variation. The artifacts together with material heterogeneity cause the object regions to exhibit a gradation of intensity values in the image. In spite of the graded composition, knowledgeable human observers usually do not have any difficulty in perceiving object regions as a gestalt. That is, image elements in these regions seem to hang together to form the object regions in spite of their gradation of values. These two notions — graded composition and hanging togetherness — must be somehow addressed by theories and strategies that aim at defining objects in acquired images.

Although hard object segmentation does not account for most of the inaccuracies and graded composition of objects in image data, a significant progress has been made in effectively visualizing, manipulating and analyzing object information captured in acquired multidimensional images in a variety of application areas.[1–3] The principle of attempting to retain data inaccuracies and object graded composition as realistically as possible in object representations derived from images, and subsequently in object visualization, manipulation and analysis, is undoubtedly the right stand. Considerable progress has been made toward this goal using fuzzy subset theory as a mathematical vehicle.[4] However, attempts to handle the notion of hanging togetherness also in the same fuzzy setting are very sparse.[5–9] We developed a framework of fuzzy connected object definition theory and algorithms.[9] In this framework, a local fuzzy relation called *affinity* is defined on the image domain which assigns to every pair of nearby image elements a strength of local hanging togetherness which has a value in [0,1]. Affinity between two elements depends on their spatial nearness as well as how similar their image intensities and intensity derived features are. Fuzzy affinity leads to a global fuzzy relation called *fuzzy connectedness* which assigns to every pair (c, d) of image elements a strength of global hanging togetherness that has a value in [0,1]. In defining a fuzzy connected object, the strength of connectedness of all possible pairs of elements is considered and solved via dynamic-programming.[9]

Correspondence: Email: saha@mipg.upenn.edu; http://www.mipg.upenn.edu/~saha/index.html; Telephone: 215 662 6780
Fax 215 898 9145

The fuzzy connectedness algorithms have been effectively utilized in several medical applications including multiple sclerosis lesion detection and quantification via MR imaging,[10] blood vessel definition in MR angiography,[11] and in the separation of bone and soft tissues from skin in CT images for craniomaxillofacial 3D visualization.[12] The fuzzy connectedness methodology has been further extended by several researchers recently.[13–16]

"Scale" is a fundamental, well-established concept in image processing.[17,18] The premise behind this concept is to consider the local size of the object in carrying out whatever local operations that are done on the image. Since affinity is a local phenomenon, in determining its strength, it makes sense to consider local scale. This can make it more robust and less sensitive to noise, and therefore, can improve the fuzzy connected object definition itself. This as the central theme, this paper makes the following contributions. (1) It presents a family of new affinity relations within the framework of the affinity relation suggested in.[9] (2) It introduces the notion of scale-based affinity and connectedness, describes a family of such relations and demonstrates that the earlier theoretical framework for fuzzy connected object definition can be readily extended to the scale-based situation. (3) It comparatively assesses the effectiveness of non scale-based and scale-based strategies in several image segmentation tasks.

In our previous fuzzy connectedness framework,[9] the affinity definition was allowed any, but fixed, neighborhood size. It did not indicate how this size was to be selected. In this paper, we relax this to a variable neighborhood size that is related to the local scale. In Section 2, we describe several new non scale-based affinity relations. In Section 3, we describe the new scale-based formulation. In Section 4, we present the algorithms for computing the local scale and for computing scale-based fuzzy connected objects. In Section 5, we describe a validation study that demonstrates that the scale-based method is indeed superior to simple fuzzy connected formulations under various conditions of noise, blurring, and background variations. In Section 6, we state our concluding remarks.

2. NON SCALE-BASED FUZZY AFFINITY

In this section, we describe a generic class of new non scale-based fuzzy affinity relations. We will follow closely the terminology, notation and formulations of Udupa and Samarasekera.[9] A more detailed version of this paper with the complete theory is available in a technical report.[19]

We consider the pair (Z^n, α) to represent a *fuzzy digital space* where Z^n is the set of n-tuples of integers and α is a *fuzzy adjacency* relation in Z^n. An element of Z^n will be called a *spel* (spatial element). In this paper, we have used the following membership function μ_α for the fuzzy adjacency relation α. For any spel c, $\mu_\alpha(c,c) = 1$. Further, for any spels c, d, $\mu_\alpha(c,d) = 1$ if c and d differ in exactly one coordinate by 1. Otherwise, $\mu_\alpha(c,d) = 0$. A *scene over* a fuzzy digital space (Z^n, α) is a pair $C = (C, f)$ where $C = \{c \mid -b_j \leq c_j \leq b_j \text{ for some } b \in Z_+^n\}$, Z_+^n is the set of n-tuples of positive integers, f is a function whose domain is C, called the *scene domain*, and whose range is a set of integers $[L, H]$. In the fuzzy connectivity approach, a strength of connectedness is determined between every pair of image elements. This is done by considering all possible connecting paths between the two elements in a pair. The strength assigned to a particular path is defined as the weakest affinity between successive pairs of elements along the path. Affinity specifies the degree to which elements hang together locally in the image. Any fuzzy relation κ in C is said to be a *fuzzy spel affinity in* C if it is reflexive and symmetric. In practice, we would want κ to be such that $\mu_\kappa(c,d)$ is a function of $\mu_\alpha(c,d)$ and of $f(c)$ and $f(d)$ and perhaps even of c and d themselves.[9] We consider that affinity should consist of two components — a *homogeneity-based component*, and an *object-feature-based component*. With this recognition, we may devise a variety of functional forms for each component separately and combine them to produce the affinity relation suited for the application on hand.

The two components are quite independent and there exist certain dichotomies between them. The object-feature-based component does not capture the notion of path homogeneity. To clarify this, consider two spels c and d that are in the same object region but that are far apart. Assume that there is a slow varying background intensity component such as what is often found in MR images due to magnetic field inhomogeneities. Spels c and d are likely to have very different scene intensities although they belong to the same object. Nevertheless, one can find a path (a sequence of nearby (say, adjacent) spels) from c to d in the scene domain such that intensities of each pair (c', d') of successive spels on the path are very similar. That is, c' and d' have a strong homogeneity-based affinity. Conversely, the homogeneity-based component alone cannot adequately capture the notion of a global agreement to known object intensity characteristics. Again consider a path from c to d along which spel intensity changes very slowly. The path may pass through different object regions. Without an object-feature-based component, this path will indicate a strong connectedness between c and d and therefore will merge the different objects it passes through into one object. We argue that, generally both the homogeneity- and object-feature-based components should be

considered in the design of fuzzy spel affinities, although in some applications each component on its own may be adequate. We express this in the following functional form for μ_κ:

$$\mu_\kappa(c,d) = \mu_\alpha(c,d)\, g(\mu_\psi(c,d), \mu_\phi(c,d)), \tag{1}$$

where μ_ψ and μ_ϕ represent the homogeneity-based and object-feature-based components of affinity, respectively. Our intuitive notion of an "object" and its intensity characteristics dictate that the function g in (1) satisfies the following properties.

1. The range of g should be [0,1].
2. g should be such that for any given μ_ψ (respectively, μ_ϕ), μ_κ should be monotonically nondecreasing with increasing μ_ϕ (respectively, μ_ψ). Roughly, it says that affinity should increase with each component.

In this paper, we use the following functional form for μ_κ

$$\mu_\kappa = \mu_\alpha \sqrt{\mu_\psi \mu_\phi}\,. \tag{2}$$

For the homogeneity-based affinity, we assume that the homogeneity (rather, the inhomogeneity) between any two spels c and d in a scene $C = (C, f)$ can be characterized by $|f(c) - f(d)|$, and express $\mu_\psi(c,d)$ as some function of $|f(c) - f(d)|$.

$$\mu_\psi(c,d) = W_\psi(|f(c) - f(d)|). \tag{3}$$

Our intuitive notion of an "object" and its intensity characteristics require that W_ψ satisfies the following properties.

1. The range of W_ψ should be [0,1], $W_\psi(0) = 1$.
2. Different object regions in different scenes have different degrees of homogeneity. Spels c and d with inhomogeneity $\Delta = |f(c) - f(d)|$ in an object with overall high homogeneity should have a smaller value for W_ψ than for spels u and v with the same inhomogeneity Δ in a scene for another object with a lower overall homogeneity.
3. W_ψ should be monotonically non-increasing with $|f(c) - f(d)|$.

In fuzzy subset theory, there are many membership functions corresponding to the fuzzy proposition "x is small" that satisfy the above requirements[20] (Page 168). In this paper, we use the following functional form for W_ψ

$$W_\psi(x) = e^{-\frac{x^2}{2k_\psi^2}}. \tag{4}$$

For the object-feature-based component of affinity, the only feature considered here is the spel intensity itself. Our treatment of μ_ϕ is somewhat different from that of μ_ψ. We will consider the object feature as well as background feature to formulate μ_ϕ. We will use an object membership function W_o as well as a background membership function W_b to capture the idea of belongingness of any spel in the respective regions, and then combine these to obtain μ_ϕ.

Any membership function corresponding to the fuzzy proposition "x is close to an expected value"[20] (Page 170) is an appropriate candidate for W_o and W_b. In this paper, we use the following functional forms for W_o, W_b

$$W_o(x) = e^{-\frac{(f(x)-m_o)^2}{2k_o^2}}, \tag{5}$$

$$W_b(x) = e^{-\frac{(f(x)-m_b)^2}{2k_b^2}}. \tag{6}$$

The parameters are subscripted to indicate their association with the object or the background. Note that m_o, m_b may lie anywhere in $[L, H]$. In particular, when $m_o = L$, only the right half of the function will exist. Similarly, when $m_o = H$, only the left half will exist.

Finally, we consider a pair of spels (c,d) to have a high object-feature-based affinity only if both c and d have high object belongingness (i.e., the value of W_o) *and* both have low background belongingness (i.e., the value of W_b). The functional form chosen to reflect this strategy is as follows:

$$\mu_\phi(c,d) = \begin{cases} \frac{\min[W_o(c),W_o(d)]}{\max[W_b(c),W_b(d)]+\min[W_o(c),W_o(d)]}, & \text{if } \min[W_o(c),W_o(d)] \neq 0, \text{ and } c \neq d, \\ 1, & \text{if } c = d, \\ 0, & \text{otherwise.} \end{cases} \tag{7}$$

By (2) defining κ, (3) & (4) defining μ_ψ, and by (5) to (7) defining μ_ϕ, we have constructed a family of fuzzy relations. The following theorems (proofs are omitted for brevity) establish that each member of this family is indeed a fuzzy spel affinity. We will denote respectively by Ψ and Φ the set of fuzzy relations in C defined by (3) and (4) and by (5)–(7). We denote by Ξ the set of all fuzzy relations constructed using (2) wherein ψ and ϕ are any elements of Ψ and Φ, respectively.

Theorem 1. For any scene $\mathcal{C} = (C,f)$ over any fuzzy digital space (Z^n,α), any $\psi \in \Psi$ and $\phi \in \Phi$ are fuzzy spel affinities in $\mathcal{C}$.

Theorem 2. For any scene $\mathcal{C} = (C,f)$ over any fuzzy digital space (Z^n,α), any fuzzy relation $\xi \in \Xi$ is a fuzzy spel affinity in $\mathcal{C}$.

3. SCALE-BASED FUZZY AFFINITY

In defining both ψ and ϕ in the previous section, we considered the intensity of just the spel under consideration. The approach in the scale-based formulation is to determine μ_ψ and μ_ϕ based on the neighborhood whose size is related to the local scale of the object. This strategy makes μ_ψ and μ_ϕ, and eventually μ_κ, less sensitive to local noise.

Roughly, *object scale in* $\mathcal{C}$ at any spel $c \in C$ is the radius $r(c)$ of the largest hyperball centered at c which lies entirely in the object region. Ironically, all this is done exactly for the purpose of defining the object in the first place and it appears that object definition is needed first to define scale. In Section 4, we will describe an algorithm which estimates $r(c)$ for any $\mathcal{C}$ without explicit object definition but based on the continuity of intensity homogeneity. Although, this estimation is not perfect, we hypothesize that this information leads to better fuzzy connectedness and object definition. For now, we assume that $r(c)$ is known at any $c \in C$. In determining the scale-based fuzzy affinity between any spels $c,d \in C$, two digital hyperballs, centered at c and d, denoted $B_{cd}(c)$, and $B_{cd}(d)$ both of radius $\min[r(c),r(d)]$, defined by

$$B_{cd}(c) = \{e \in C \mid \|c-e\| \leq \min[r(c),r(d)]\}, \tag{8}$$

$$B_{cd}(d) = \{e \in C \mid \|d-e\| \leq \min[r(c),r(d)]\}, \tag{9}$$

where $\|\cdot\|$ denotes the Euclidean distance. As in the non scale-based case, we will keep the homogeneity- and object-feature-based components separate, and denote them by ψ_s and ϕ_s, respectively.

3.1. The Homogeneity-Based Component

Consider any two spels $c,d \in C$ such that $\mu_\alpha(c,d) > 0$. Consider any spels $e \in B_{cd}(c)$ and $e' \in B_{cd}(d)$ such that they represent the corresponding spels within $B_{cd}(c)$ and $B_{cd}(d)$, that is $c-e = d-e'$. We will define two weighted sums $D^+(c,d)$ and $D^-(c,d)$ of differences of intensities between the two balls as follows.

$$\delta^+_{cd}(e,e') = \begin{cases} f(e)-f(e'), & \text{if } f(e)-f(e') > 0, \\ 0, & \text{otherwise,} \end{cases} \tag{10}$$

$$\delta^-_{cd}(e,e') = \begin{cases} f(e')-f(e), & \text{if } f(e)-f(e') < 0, \\ 0, & \text{otherwise,} \end{cases} \tag{11}$$

and

$$D^+(c,d) = \sum_{\substack{e \in B_{cd}(c) \\ e' \in B_{cd}(d) \\ \text{s.t. } c-e=d-e'}} [1 - W_{\psi_s}(\delta^+_{cd}(e,e'))]\,\omega_{cd}(\|c-e\|), \tag{12}$$

$$D^-(c,d) = \sum_{\substack{e \in B_{cd}(c) \\ e' \in B_{cd}(d) \\ \text{s.t. } c-e=d-e'}} [1 - W_{\psi_s}(\delta^-_{cd}(e,e'))]\,\omega_{cd}(\|c-e\|). \tag{13}$$

W_{ψ_s} and ω_{cd} are window functions which have the same requirements as those specified for W_ψ of (3) described in Section 2. We will therefore use the same functional forms depicted in (4). We note that the parameter $k_{w_{cd}}$ of ω_{cd} depends on $r(c)$ and $r(d)$ as illustrated in Section 5.1.

The connection of the above equations to the homogeneity-based affinity is as follows. There are two types of intensity variations surrounding c and d — intra- and inter-object variations. The intra-object component is generally random, and therefore, is likely to be near 0 overall. The inter-object component, however, has a direction. It either increases or decreases along the direction given by $c-d$, and is likely to be larger than the intra-object variation. It is reasonable, therefore, to assume that the smaller of $D^+(c,d)$ and $D^-(c,d)$ represents the intra-object component and the other represents the combined effect of the two components. (Note that when the values of δ^+_{cd} (respectively, δ^-_{cd}) are small, $D^+(c,d)$ (respectively, $D^-(c,d)$) also becomes small.) Note that, if there is a slow background component of variation, within the small neighborhood considered, this component is unlikely to cause a variation comparable to the inter-object component. This strategy leads us to the following functional form for μ_{ψ_s}:

$$\mu_{\psi_s}(c,d) = 1 - \frac{|D^+(c,d) - D^-(c,d)|}{\sum_{e \in B_{cd}(c)} \omega_{cd}(\|c-e\|)}. \tag{14}$$

Note that $|D^+(c,d) - D^-(c,d)|$ represents the degree of local inhomogeneity of the regions containing c and d. Its value is low when both c and d are inside an (homogeneous) object region. Its value is high when c and d are in the vicinity of (or across) a boundary. The denominator in (14) is a normalization factor.

3.2. The Object-Feature-Based Component

The formulation of ϕ_s is analogous to that of ϕ with one difference. Instead of considering directly the spel intensities $f(c)$, we will consider a filtered version of it that takes into account the ball $B_r(c)$ at c defined by

$$B_r(c) = \{e \in C \mid \|c-e\| \le r(c)\}. \tag{15}$$

The filtered value at any $c \in C$ is given by

$$f_a(c) = \frac{\sum_{e \in B_r(c)} f(e)\,\omega_c(\|c-e\|)}{\sum_{e \in B_r(c)} \omega_c(\|c-e\|)}, \tag{16}$$

where ω_c is as described in Section 3.1 and the parameter k_{w_c} depends on $r(c)$. The functional forms for defining μ_{ϕ_s} are exactly as in (4)–(7) that defined μ_ϕ except that $f(c)$ and $f(d)$ are replaced by $f_a(c)$ and $f_a(d)$. We will denote the scale-based versions of W_o and W_b by W_{os} and W_{bs}, respectively.

$$\mu_{\phi_s}(c,d) = \begin{cases} \frac{\min[W_{os}(c), W_{os}(d)]}{\max[W_{bs}(c), W_{bs}(d)] + \min[W_{os}(c), W_{os}(d)]}, & \text{if } \min[W_{os}(c), W_{os}(d)] \neq 0, \text{ and } c \neq d, \\ 1, & \text{if } c = d, \\ 0, & \text{otherwise.} \end{cases} \tag{17}$$

Finally, the scale-based versions κ_s of the relations expressed in (2) are obtained by replacing ψ and ϕ in that equation by ψ_s and ϕ_s. As in the non scale-based case, we denote by Ψ_s, Φ_s and Ξ_s the three sets of all possible ψ_s, ϕ_s and κ_s constructed as described in Sections 3.1 and 3.2. The following theorems establish that these scale-based fuzzy relations are indeed fuzzy spel affinities.

Theorem 3. For any scene $\mathcal{C} = (C, f)$ over any fuzzy digital space (Z^n, α), any $\psi_s \in \Psi_s$ and $\phi_s \in \Phi_s$ are fuzzy spel affinities in $\mathcal{C}$.

Theorem 4. For any scene $\mathcal{C} = (C, f)$ over any fuzzy digital space (Z^n, α), any fuzzy relation $\xi_s \in \Xi_s$ is a fuzzy spel affinity in $\mathcal{C}$.

4. ALGORITHMS

In this section, we first describe an algorithm which produces the object scale $r(c)$ for any spel c in a given scene. This will be followed by a presentation of the scale-based fuzzy connectedness algorithm.

4.1. Computation of Scale

For a ball $B_k(c)$ of any radius k (see (15)) centered at c, we define a fraction, $FO_k(c)$, that indicates the fraction of the ball boundary occupied by a region which is sufficiently homogeneous with c, by

$$FO_k(c) = \frac{\sum_{d \in B_k(c) - B_{k-1}(c)} W_{\psi_s}(|f(c) - f(d)|)}{|B_k(c) - B_{k-1}(c)|}, \tag{18}$$

where W_{ψ_s} is the homogeneity function used for defining ψ. Note that $B_0(c)$ is the set $\{c\}$. The algorithm for object scale estimation is summarized below.

Algorithm *OSE*
Input: $\mathcal{C}$, $c \in C, W_{\psi_s}$, a fixed threshold t_s.
Output: $r(c)$.
begin
    set $k = 1$;
    while $FO_k(c) \geq t_s$ *do*
        set k to $k + 1$;
    endwhile;
    set $r(c)$ to k;
    output $r(c)$;
end

The algorithm iteratively increases the ball radius k by 1, starting from 1, and checks for the fraction of the object $FO_k(c)$ containing c that is contained on the ball boundary. The first time when this fraction falls below t_s, we consider that the ball enters into an object region different from that to which c belongs. In our experiments in this paper, we have used $t_s = 0.85$. The rationale for this choice is as follows. In a $3 \times 3 \times 3$ neighborhood of a voxel c in a 3D scene $\mathcal{C}$, we allow one out of the six neighboring voxels to belong to a different object (to account for noise) and still consider the neighborhood to be entirely within the same object. This leads to $t_s = \frac{5}{6}$. We did not notice any change in the results by varying t_s in [0.8, 0.9].

For completeness, we will give a brief description of the fuzzy connectedness relation. For details see.[9] Let κ be any fuzzy spel affinity in C. Fuzzy connectedness is a fuzzy relation K in C that assigns to every pair (c, d) of spels in C a number $\mu_K(c, d)$ in $[0, 1]$ as follows. Consider any path (a sequence of nearby spels) from c to d in C. The "strength of connectedness" of this path is simply the smallest affinity of pairwise spels in the path. $\mu_K(c, d)$ is simply the largest of the strengths of connectedness of all possible paths between c and d.

The scale-based fuzzy connectedness algorithm is presented below. In fact, there is nothing special about it being scale-based. It works for any fuzzy spel affinity, scale-based as well as non scale-based. For any spel affinity κ in a scene $\mathcal{C} = (C, f)$ over a fuzzy digital space (Z^n, α), we define the *κ-connectivity scene $\mathcal{C}_{Ko}$ of $\mathcal{C}$ with respect to a spel* $o \in C$ by $\mathcal{C}_{Ko} = (C, f_{Ko})$, where, for any $c \in C$, $f_{Ko}(c) = \mu_K(o, c)$. That is, the spel intensities in $\mathcal{C}_{Ko}$ represent the strength of connectedness of the spels with respect to o. The algorithm uses dynamic programming[21] to find the best path from o to each spel in C. See[9] for further details on this and related algorithms. We reproduce here the main algorithm for completeness. The fuzzy connected object of a certain strength θ containing the spel o is obtained by thresholding $\mathcal{C}_{Ko}$ at θ.[9]

Algorithm *κFOE*
Input: $\mathcal{C} = (C, f)$, any $o \in C$ and any fuzzy spel affinity κ in $\mathcal{C}$.
Output: A κ-connectivity scene $\mathcal{C}_{Ko} = (C, f_{Ko})$ of $\mathcal{C}$ with respect to o.
Auxiliary Data Structures: An n-D array representing the connectivity scene $\mathcal{C}_{Ko} = (C, f_{Ko})$ of $\mathcal{C}$ and a queue Q of spels. We refer to the array itself by $\mathcal{C}_{Ko}$ for the purpose of the algorithm.

begin

set all elements of C_{Ko} to 0 except o which is set to 1;
push all spels $c \in C$ such that $\mu_\kappa(o,c) > 0$ to Q;
while Q is not empty *do*
remove a spel c from Q;
find $f_{\max} = \max_{d \in C}[\min(f_{Ko}(d), \mu_\kappa(c,d))]$;
if $f_{\max} > f_{Ko}(c)$ *then*
set $f_{Ko}(c) = f_{\max}$;
push all spels e such that $\mu_\kappa(c,e) > 0$ to Q;
endif;
endwhile;

end

That this algorithm terminates and at that time it indeed outputs the κ-connectivity scene C_{Ko} of C has been proved in.[9]

5. EXPERIMENTS AND VALIDATION

The parameters associated with ψ, ϕ, ψ_s, and ϕ_s allow many possible choices for scale-based and non scale-based fuzzy spel affinities. In Section 5.1, we describe our experimental studies for getting some insight into the choice of different parameters. Based on these selections, the non scale-based and scale-based methods are compared qualitatively through 2D and 3D segmentations in Section 5.2. A formal comparison based on a set of image phantoms is made in Section 5.3 to quantitatively assess the relative performance of the two methods.

5.1. Selection of Parameters

To visually assess the goodness of a fuzzy spel affinity κ in a scene $C = (C, f)$, we represent the membership values of κ as a *κ-affinity scene of C*, denoted $C_\kappa = (C, f_\kappa)$, defined as follows. For any spel $c \in C$,

$$f_\kappa(c) = \frac{1}{|N(c)|} \sum_{d \in N(c)} \mu_\kappa(c,d), \tag{19}$$

where

$$N(c) = \{d \in C \mid \text{ for } 1 \le i \le n,\ d_i - c_i \ge 0,\ c \ne d, \text{ and } \mu_\alpha(c,d) > 0\}. \tag{20}$$

Each spel c in C_κ has a value which is the average of the affinity values of c with other spels in its neighborhood which are in the positive coordinate direction with respect to c. However, in actual segmentation, the affinity is defined with respect to all neighbors in the nD scene and the affinity scene does not play any role.

Another tool we use in the selection of parameters is training. In our implementation, an operator paints, on a display of a slice of the scene, regions of the object and of the background using a mouse-controlled brush. The mean (M_o, M_b) and the standard deviation (σ_o, σ_b) of the intensities in the painted object and the background region are computed. Similarly, the mean (M_h) and the standard deviation (σ_h) of inhomogeneity in the object region are computed as the mean and standard deviation of intensity differences $|f(c) - f(d)|$ for all possible pairs (c,d) of spels in the painted object region such that $c \ne d$ and $\mu_\alpha(c,d) > 0$. These estimated parameters are used in setting up the values of the parameters of $\mu_\psi, \mu_\phi, \mu_{\psi_s}$, and μ_{ϕ_s} as indicated below.

$\underline{\mu_\psi}$: $k_\psi = M_h + t\,\sigma_h$.

$\underline{\mu_\phi}$: $m_o = M_o$, $k_o = t\,\sigma_o$, $m_b = M_b$, $k_b = t\,\sigma_b$.

In these expressions, t is set to a number between 2 and 3. (The rationale for this is that in a normal distribution, 2–3 standard deviations on the two sides of the mean cover 95.4–99.7 of the population.) For μ_{ψ_s}, the parameters are set as above for μ_ψ, and for μ_{ϕ_s}, they are set as above for μ_ϕ. For ω_{cd} and ω_c, the parameters are not spatially invariant; rather they depend on the local scale size at c and d as follows.

$\underline{\omega_{cd}}$: $k_{\omega_{cd}} = \min[r(c), r(d)]$.

$\underline{\omega_c}$: $k_{\omega_c} = r(c)$.

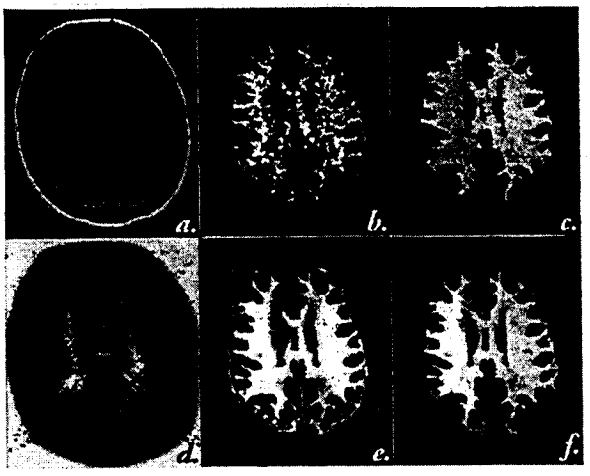

Figure 1. (a). An MR slice of a patient's head. (b), (e). Affinity scenes obtained for the slice in (a) using non scale-based and scale-based fuzzy affinity relations, respectively. (c), (f). The connectivity scenes obtained for the spel affinities illustrated in (b), (e), respectively. The starting pixel is specified in the left middle part of the white matter region. (d). The scale value $r(c)$ for the image in (a), is shown as an image.

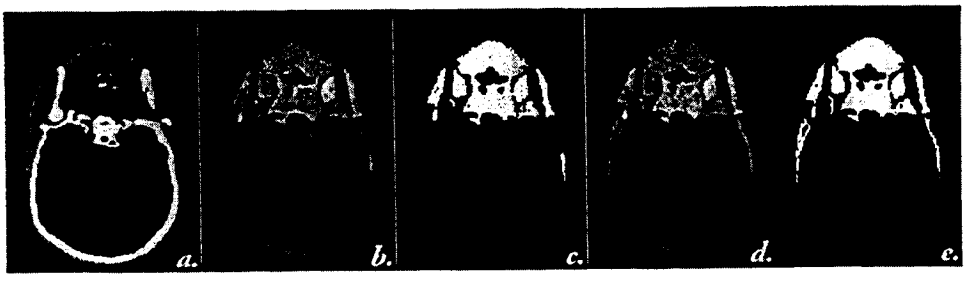

Figure 2. (a). A 2D scene representing a slice of a CT scene of a patient's head. (b), (d). The connectivity scenes obtained for the scene in (a) via non scale-based and scale-based methods. (c), (e). The fuzzy objects obtained for the scene in (a) via non scale-based and scale-based methods for optimum thresholds chosen interactively in both cases.

Figure 1(a) shows a slice of a 3D MR proton density weighted scene of a patient's head. Figures 1(b) and (c) show an affinity and a connectivity scene obtained using the non scale-based method and the parameters selected as above for the slice shown in Figure 1(a). Figure 1(d) shows the object scale information as a 2D scene for the slice in Figure 1(a). Figures 1(e) and (f) show an affinity and a connectivity scene obtained using the scale-based method and the parameters selected as above for the slice shown in Figure 1(a). In both cases, the same starting pixel was used and it was specified on the left middle part of the white matter region for determining the connectivity scenes.

5.2. Qualitative Comparison

In this section, we present one 2D (Figure 2) and one 3D (Figure 3) examples comparing the non scale-based with the scale-based method. In all examples, the same spels were specified as starting information for both methods. Figure 2(a) shows a slice of a CT scene of a patient's head. Our aim here is to segment the soft tissues (the muscles) excluding the skin as much as possible. The muscles appear with intermediate brightness in Figure 2(a). The skin appears with almost the same brightness and surrounds the cross section with a thin boundary of a width of a few pixels.

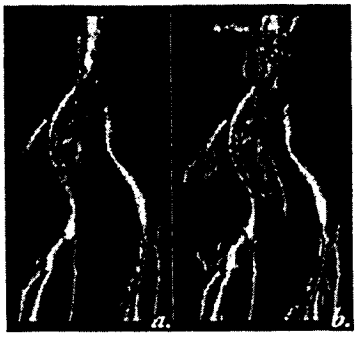

Figure 3. 3D renditions of the fuzzy objects (the vascular tree) extracted from an MR angiographic 3D scene via non scale-based (a) and scale-based (b) methods. The same single voxel was specified in the main body of the vessel as the starting spel in both cases.

Figures 2(b) and (c) show the connectivity scene and the fuzzy object obtained via the non scale-based method. Figures 2(d) and (e) show the connectivity scene and the fuzzy object obtained via the scale-based method. In both cases, the best threshold to obtain the fuzzy object was selected interactively. Figure 3 illustrates 3D renditions of the fuzzy objects (vessel) extracted from an MR angiographic scene. The fuzzy object information is rendered via 3DVIEWNIX[22] supported shell rendering method.[23] The MR angiography scene has a domain of 256 × 256 × 128 and a voxel size of 1.09mm. × 1.09mm. × 2.20mm.

In both the 2D and 3D examples given above , we observe that the scale-based method produces more accurate segmentation than the non scale-based method. It picks up fewer spurious regions and seems to produce clearer segmentation than the latter. Subtle and small aspects of the objects are better delineated and differentiated from noise. This is evident in the renditions of the vessels where some thin branches are lost in the non scale-based method. In the craniofacial example, both methods effectively separate the skin from the muscles. The scale-based method (Figures 2(d),(e)) has captured all segments of the muscles while the non scale-based method lost some.

5.3. Quantitative Comparison

The image phantoms used in our objective comparison of non scale-based and scale-based methods are generated from 10 different patient MR studies of the brain. One transaxial slice, approximately at the same location in the brain is selected from each of these 10 3D scenes. Each of these 10 2D scenes is segmented carefully to separate the white matter and brain parenchymal regions using a user steered segmentation method.[24] From this information, from each of the original 10 2D scenes, a new 2D scene is generated by assigning to pixels in each region a constant intensity equal to the average of the intensities within the same segmented region in the corresponding original MR 2D scene. From this set of 10 simulated 2D scenes, we created a total of 250 2D scenes, $E = \{C_i \mid C_i = (C, f_i), 1 \leq i \leq 250\}$, by blurring (using a 2D Gaussian kernel) each 2D scene in this set to five different degrees of blurring and by adding a 0-mean Gaussian correlated noise at five different levels and by adding a fixed slow varying (ramp) background component from 0 to 100 across the column.

Let $E_b = \{C_{bi} \mid C_{bi} = (C, f_{bi}), 1 \leq i \leq 250\}$ be the set of binary scenes such that, for $1 \leq i \leq 250$, C_{bi} represents the original segmentation of the white matter region corresponding to the simulated scene C_i in E. We denote by $E_s = \{C_{si} \mid C_{si} = (C, f_{si}), 1 \leq i \leq 250\}$ and $E_{ns} = \{C_{nsi} \mid C_{nsi} = (C, f_{nsi}), 1 \leq i \leq 250\}$ the set of connectivity scenes produced by the scale-based and non scale-based methods, respectively, from the set E of input scenes.

In the following, for any scene $C = (C, f)$, we denote by $C^t = (C, f^t)$ the binary scene resulting from thresholding C at t. That is, for any $c \in C$

$$f^t(c) = \begin{cases} 1, & \text{if } f(c) \geq t, \\ 0, & \text{otherwise.} \end{cases}$$

We define figures of merit FOM_{si} and FOM_{nsi} for the accuracy of segmentation for the scale-based and non scale-based methods as follows. For $x \in \{s, ns\}$, and $1 \leq i \leq 250$,

$$FOM_{xi} = \max_t \left[\left(1 - \frac{|C_{xi}^t \; EOR \; C_{bi}|}{|C_{bi}|} \right) \times 100 \right], \tag{21}$$

where $|\mathcal{Y}|$ denotes the number of 1-valued pixels in the scene denoted by $\mathcal{Y}$ and EOR represents the Exclusive OR operation between the two binary scenes. For method x, FOM_{xi} represents the best possible degree of match between the original (true) white matter object region captured in C_{bi} and the white matter object region in C_{xi} over all possible thresholds t on C_{xi}. In this fashion, our comparison becomes independent of how the connectivity scenes are thresholded.

Table 1. The mean and standard deviation of FOM_{nsi} values are shown in each cell for different blurring and noise conditions.

	blur 1	*blur* 2	*blur* 3	*blur* 4	*blur* 5
noise 1	98.20	97.45	96.66	94.91	93.39
	0.16	0.26	0.41	0.65	0.89
noise 2	98.29	97.36	96.42	94.56	93.02
	0.08	0.21	0.36	0.77	0.94
noise 3	98.11	96.95	95.94	94.06	92.49
	0.11	0.28	0.43	0.87	0.96
noise 4	96.69	95.33	94.21	92.37	90.93
	0.37	0.72	0.77	1.20	1.13
noise 5	94.30	92.84	91.76	90.20	89.03
	1.59	1.47	1.54	1.59	1.29

Table 2. The mean and standard deviation of FOM_{si} values are shown in each cell for different blurring and noise conditions.

	blur 1	*blur* 2	*blur* 3	*blur* 4	*blur* 5
noise 1	99.25	98.32	97.43	95.84	94.35
	0.02	0.10	0.23	0.55	0.83
noise 2	99.13	98.14	97.21	95.43	93.86
	0.02	0.12	0.25	0.61	0.99
noise 3	98.83	97.70	96.74	94.98	93.50
	0.04	0.16	0.35	0.70	1.03
noise 4	97.85	96.70	95.71	93.67	91.83
	0.15	0.29	0.50	0.77	1.03
noise 5	96.41	95.18	94.20	91.24	89.46
	0.50	0.60	0.75	1.02	1.26

Tables 1 and 2 list in each cell the mean and the standard deviation of FOM_{nsi} and FOM_{si}, respectively, for each degree of blurring and noise for the 10 scenes. Table 3 lists the mean difference of the FOM values for the methods for the different degrees of blurring and noise. A paired Student t test[25] of the 10 pairs of FOM data for each degree of blurring and noise was conducted under the null hypothesis that there is no statistical difference between the two methods. The hypothesis was rejected at a very high level of confidence ($p < 10^{-3}$) in all 25 tests.

We observe from Table 3 that the scale-based method achieves better relative performance as noise increases. This can be seen by examining the entries in each column in Tables 1 and 2. At very high degrees of blurring and noise, the two methods perform more-or-less equally badly. When the blurring is not too high so that object scale can be estimated reasonably accurately, the scale based method clearly shows a superior performance and its robustness to noise.

Table 3. Mean of $FOM_{nsi} - FOM_{si}$ over the 10 scenes for different degrees of blurring and noise. A paired Student's t test indicates that this mean difference is significant with $p < 0.001$ in all the 25 cases.

	blur 1	*blur* 2	*blur* 3	*blur* 4	*blur* 5
noise 1	1.053	0.867	0.775	0.935	0.951
noise 2	0.842	0.774	0.790	0.870	0.844
noise 3	0.719	0.749	0.797	0.916	1.002
noise 4	1.159	1.374	1.505	1.304	0.900
noise 5	2.105	2.347	2.438	1.044	0.434

6. CONCLUDING REMARKS

Based on a previously developed framework of fuzzy connectedness and object definition in multi-dimensional scenes,[9] we have proposed an extension of this framework that takes into account the local object size in defining connectedness. There are three fundamental premises on which this development is based. (1) The fuzziness inherent in acquired scenes stemming from object material inhomogeneity, noise, blurring, and background variations must be properly accounted for. (2) The local object size must be taken into account in determining how spatial elements of the scene locally hang together, that is, in determining their affinity. (3) Two separate aspects of the affinity between spels must be considered — the homogeneity-based and object-feature-based components.

We have presented a process of constructing a family of new affinity relations and have also shown how to include object scale information in this process for constructing a family of scale-based affinity relations. We have demonstrated that the original theoretical and algorithmic framework is valid also for the new non scale-based and scale-based affinities. Based on 250 image phantoms generated under a range of conditions of blurring, noise and background variation, our comparison of the non scale-based and scale-based methods indicates a definite superiority of the scale-based connectedness method over the new non scale-based connectedness strategies.

The non scale-based algorithm takes about 20 minutes on a SUN Sparc 20 workstation to detect an object such as the brain in a $256 \times 256 \times 60$ scene. The scale-based method takes about 45 minutes for the same task. Although we have not focussed on optimization of the algorithms, others have demonstrated[14] roughly an 8-fold speed up on 2D scenes with certain optimizations of the original algorithm in.[9] It remains to be seen whether a similar speed up can be achieved in 3D, especially for the scale-based case.

Instead of the variable-scale approach proposed in this paper, a multi-scale approach, commonly taken in computer vision research,[26] may also be pursued. In the context of the definition of fuzzy connectedness, we felt that the variable-scale approach is more natural.

Instead of just intensity only for defining ϕ, other intensity-based features, such as texture, may also be used. If the affinity is carefully devised, the theory will hold good for other features also.

We have used the original fuzzy connectedness method to-date on over 1,500 3D patient studies in several applications involving MR brain image analysis and MR angiography. The consequence of the improved ability of the scale-based approach in these and other applications are currently being investigated.

Finally, one of the drawbacks of the current fuzzy connectedness (both scale-based and non scale-based) approach is having to select a threshold for the connectivity scene. In applications involving a large number of studies based on a fixed image acquisition protocol, the threshold (as well as the affinity parameters) can be fixed without requiring (and allowing) per-case adjustment. One alternative is to use the many automatic threshold selection methods that are available in the literature.[27] Another, the one we are pursuing, is through the relative connectedness of objects. The idea is that every spel in the scene domain has a strength of connectedness with respect to each object in the scene, background also being one object. The spel under question is grabbed by that object with respect to which it has the strongest connectedness.

ACKNOWLEDGMENTS

The authors are grateful to Drs. Grossman, Holland, and Hemmy for the brain, vessel, and the CT image data sets. The work of the authors is supported by grants DAMD 179717271 and NS 37172.

REFERENCES

1. R. Kasturi and R C. Jain, *Computer Vision: Advances & Applications*, IEEE Computer Society Press, Los Alamitos, CA, 1991.
2. J. K. Udupa, and G. T. Herman (Eds.), *3D Imaging in Medicine*, CRC Press, Boca Raton, FL, 1991.
3. R. H. Taylor, S. Lavallée, G. C. Burdea, R. Mösges (Eds.), *Computer-Integrated Surgery*, The MIT Press, Cambridge, England, 1996.
4. J. C. Bezdek and S. K. Pal, *Fuzzy Models for Pattern Recognition*, IEEE Press, New York, NY, 1992.
5. A. Rosenfeld, "Fuzzy digital topology", *Inform. Control*, **40**, pp. 76–87, 1979.
6. A. Rosenfeld, "The fuzzy geometry of image subsets", *Pattern Recognit. Lett.*, **2**, pp. 311–317, 1991.
7. I. Bloch, "Fuzzy connectivity and mathematical morphology", *Pattern Recognit. Lett.*, **14**, pp. 483–488, 1993.
8. S. Dellepiane and F. Fontana, "Extraction of intensity connectedness for image processing" *Pattern Recognit. Lett.*, **16**, pp. 313–324, 1995.
9. J. K. Udupa, and S. Samarasekera, "Fuzzy connectedness and object definition: theory, algorithms, and applications in image segmentation", *Graphical Models and Image Processing*, **58**, pp. 246–261, 1996.
10. J. K. Udupa, L. Wei, S. Samarasekera, Y. Miki, M. A. van Buchem, and R. I. Grossman, "Multiple sclerosis lesion quantification using fuzzy connectedness principles", *IEEE Trans. on Medical Imaging*, **16**, pp. 598–609, 1997.
11. J. K. Udupa, D. Odhner, J. Tian, G, Holland, and L. Axel, "Automatic clutter-free volume rendering for MR angiography using fuzzy connectedness", *SPIE Proceedings*, **3034**, pp. 111–119, 1997.
12. J. K. Udupa, J. Tian, D. Hemmy, and P. Tessier, "A pentium PC-based craniofacial 3D imaging and analysis system", *Journal of Craniofacial Surgery*, **8**, pp. 333–339, 1997.
13. T. N. Jones, *Image-Based Ventricular Blood Flow Analysis*, Doctoral Dissertation, University of Pennsylvania, Philadelphia, PA, September, 1998.
14. B. M. Carvalho, C. J. Gau, G.T. Herman, and T.Y. Kong, "Algorithms for fuzzy segmentation", *Pattern Analysis and Applications*, to appear.
15. T. N. Jones, and D. N. Metaxas, "Automated 3D segmentation using deformable models and fuzzy affinity", *Proceedings of Information Processing in Medical Imaging*, pp. 113–126, 1997.
16. C. Xu, D. Pham, and J. Prince, "Finding the brain cortex using fuzzy segmentation, isosurfaces, and deformable surface models", *Proceedings of Information Processing in Medical Imaging*, pp. 113–126, 1997.
17. M. Tabb and N. Ahuja, "Multiscale image segmentation by integrated edge and region detection", *IEEE Trans. Image Processing*, **6**, pp. 642–655, 1997.
18. T. Lindeberg, *Scale-Space Theory in Computer Vision*, Boston, MA: Kluwer, 1994.
19. P.K. Saha, J. K. Udupa, and D. Odhner, "Scale-based fuzzy connected image segmentation: theory, algorithms and validation", Technical Report-MIPG238, Medical Image Processing Group, Department of Radiology, University of Pennsylvania, Philadelphia, 1998.
20. A, Kaufmann, *Introduction to the Theory of Fuzzy Subsets*, **1**, Academic Press, New York, 1975.
21. T. Cormen, C. Leiserson, and R. Rivest, *Introduction to Algorithms*, McGraw-Hill, New York, 1991.
22. J. K. Udupa, D. Odhner, S. Samarasekera, R. Goncalves, K. Iyer, K. Venugopal, and S. Furie, "3DVIEWNIX: An open, transportable, multidimensional, multimodality, multiparametric imaging software system, *SPIE Proceedings* **2164**, pp. 58–73, 1994.
23. J. K. Udupa, and D. Odhner, "Shell rendering", *IEEE Computer Graphics and Applications*, **13**, pp. 58–67, 1993.
24. A.X. Falcão, J. K. Udupa, S. Samarasekera, and S. Sharma, "User-steered image segmentation paradigms: live wire and live lane", *Graphical Models Image Processing*, **60**, pp. 233–260, 1998.
25. B. Ronser, *Fundamentals of Biostatistics*, New York, NY: Duxbury Press, 1995.
26. L. M. Lifshitz, S. M. Pizer, "A multiresolution hierarchical approach to image segmentation based on image extrema" *IEEE Trans. Pattern Analysis Machine Intelligence*, **12**, pp. 529–540, 1990.
27. C. K. Leung, and F. K. Lam, "Maximum segmented image information thresholding", *Graphical Models Image Processing*, **60**, pp. 57–76, 1998.